Self-Adaptive Generalized S-Transform and Its Application in Seismic Time–Frequency Analysis

Naihao Liu, Jinghuai Gao, *Member, IEEE*, Bo Zhang, Qian Wang, and Xiudi Jiang

***Abstract*— Achieving a proper time–frequency (TF) resolution is the key to extract information from seismic data using TF algorithms and characterize reservoir properties using decomposed frequency components. The generalized S-transform (GST) is one of the most widely used TF algorithms. However, it is difficult to choose an optimized parameter set for the whole seismic data set. In this paper, we propose to set the parameters of the GST adaptively using the instantaneous frequency (IF) of seismic traces. Our workflow begins with building a relationship between the parameter set of the GST and IF using a synthetic wedge model. We use the IF as an indicator for the time thickness of each trace in the wedge model. We then compute the TF spectrum of each trace using the GST with different parameter sets and compare the similarity between the computed TF spectrum and theory TF spectrum. The parameter set with the largest similarity is regarded as the best parameter set for each trace in the wedge model. In this manner, we build a relationship between the parameter set and IF value. We can finally choose the optimum parameter set for the GST according to the IF values of seismic traces. We name the proposed workflow as the self-adaptive GST (SAGST). To demonstrate the validity and effectiveness of the proposed SAGST, we apply it to synthetic seismic traces and field data. Both synthetic and real data examples illustrate that the SAGST can obtain a TF representation with a high TF resolution.**

***Index Terms*— Generalized S-transform (GST), instantaneous frequency (IF), ST, self-adaptive GST (SAGST), time–frequency (TF) resolution.**

Manuscript received May 8, 2018; revised November 21, 2018 and March 8, 2019; accepted May 8, 2019. This work was supported in part by the Major Research Plan of the National Natural Science Foundation of China under Grant 91730306, in part by the National Postdoctoral Program for Innovative Talents under Grant BX201900279, in part by the Fundamental Research Funds for the Central Universities under Grant xjh012019030, in part by the National Natural Science Foundation of China under Grant 61501366, in part by the Ministry of Science and Technology of China through the National Key Research and Development Program under Grant 2018YFC0603500 and Grant 2018YFC0603501, and in part by the Major National Science and Technology Projects under Grant 2016ZX05024-001-007 and Grant 2017ZX050609. *(Corresponding author: Jinghuai Gao.)*

N. Liu is with the School of Electronic and Information Engineering, Xi'an Jiaotong University, Xi'an 710049, China, also with the National Engineering Laboratory for Offshore Oil Exploration, Xi'an 710049, China, and also with the Department of Geological Sciences, University of Alabama, Tuscaloosa, AL 35487 USA (e-mail: naihao_liu@mail.xjtu.edu.cn).

J. Gao is with the School of Electronic and Information Engineering, Xi'an Jiaotong University, Xi'an 710049, China, and also with the National Engineering Laboratory for Offshore Oil Exploration, Xi'an 710049, China (e-mail: jhgao@mail.xjtu.edu.cn).

B. Zhang is with the Department of Geological Sciences, University of Alabama, Tuscaloosa, AL 35487 USA (e-mail: bzhang33@ua.edu).

Q. Wang is with the School of Mathematics and Statistics, Xi'an Jiaotong University, Xi'an 710049, China, and also with the National Engineering Laboratory for Offshore Oil Exploration, Xi'an 710049, China (e-mail: wqlq668930@126.com).

X. Jiang is with the Geophysics Key Laboratory, Technology R&D Center, Research Institute of China National Offshore Oil Corporation (CNOOC), National Engineering Laboratory for Offshore Oil Exploration, Beijing 100029, China (e-mail: jiangxd2@cnooc.com.cn).

Color versions of one or more of the figures in this paper are available online at http://ieeexplore.ieee.org.

Digital Object Identifier 10.1109/TGRS.2019.2916792

I. Introduction

TIME-FREQUENCY (TF) analysis transforms a seismic trace in the time domain into a 2D TF plane, which evaluates and characterizes the frequency-dependent response of subsurface rocks and reservoirs [1]. TF analysis methods can be classified into four categories. The first category is the linear TF transform. The commonly linear TF transform algorithms include the Gabor transform (GT) [2], short-time Fourier transform (STFT) [3]–[5], continuous wavelet transform (CWT) [6], [7], and S-transform (ST) [8]. The linear TF transform is simple and easy to be implemented but suffers from Heisenberg's uncertain principle. The second category is based on the quadratic TF transforms, such as the Wigner–Ville distribution (WVD) [9], [10]. The quadratic-based approaches achieve a high TF resolution. However, the TF result computed using quadratic methods is interfered by the cross terms and leads to negative influences to multicomponent signal analysis [11]. The third category is based on the least-square approaches, such as the matching pursuit (MP) algorithm [12], [13] and other sparsity-promoting inversion methods [14]. The least square-based approaches aim to overcome the window effect of projection methods [15]. The high computation cost is one of the main shortages of the least square-based TF decompositions. The last category is the reassignment method [16], such as the synchrosqueezing-based transforms [17], [18]. The reassignment-based methods obtain an excellent energy concentration but suffer from expensive calculation time and are sensitive to noise [19].

The ST proposed by Stockwell *et al.* [8] is regarded as a hybrid of the STFT and CWT [20]. The ST produces a frequency-dependent resolution by setting the time window as a function of frequency [21]. The ST produces a high time resolution at high frequencies and obtains a high-frequency resolution at low frequencies. One of the advantages of the ST is that it computes the TF spectrum using the Fourier transform. Also, this property makes it very easy to reconstruct the analyzed signal using the reverse ST. However, there is

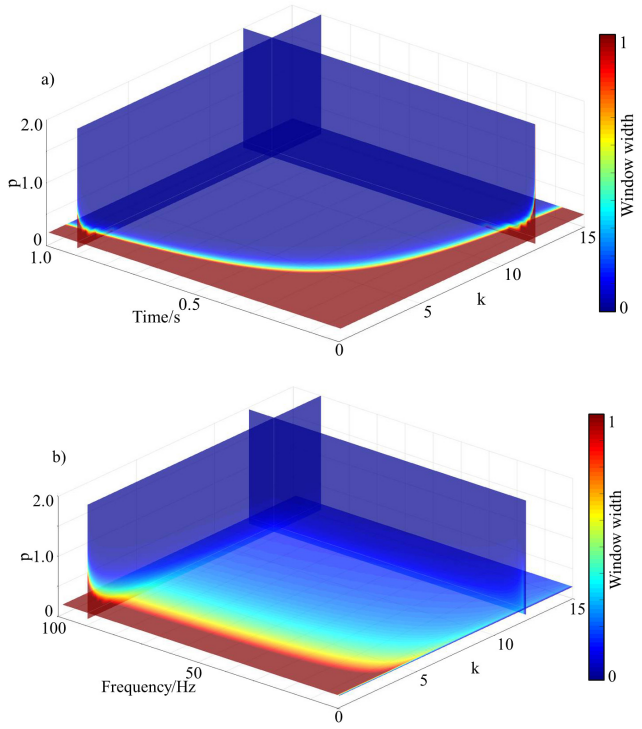

Fig. 1. Window width of the modified window with different parameters set in (a) time and (b) frequency domain, respectively. The maximum width of the window has been normalized to 1.

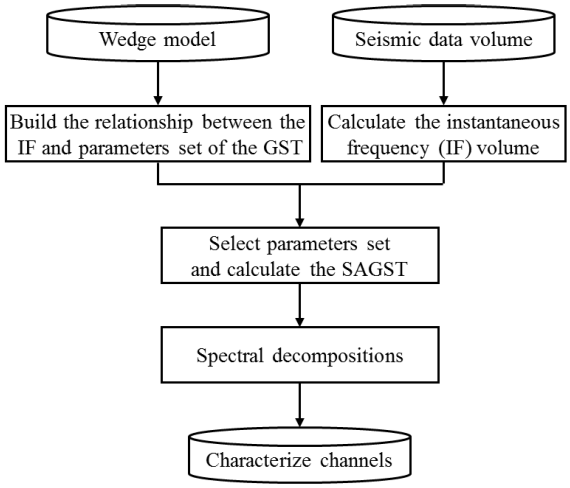

Fig. 2. Workflow of the proposed SAGST.

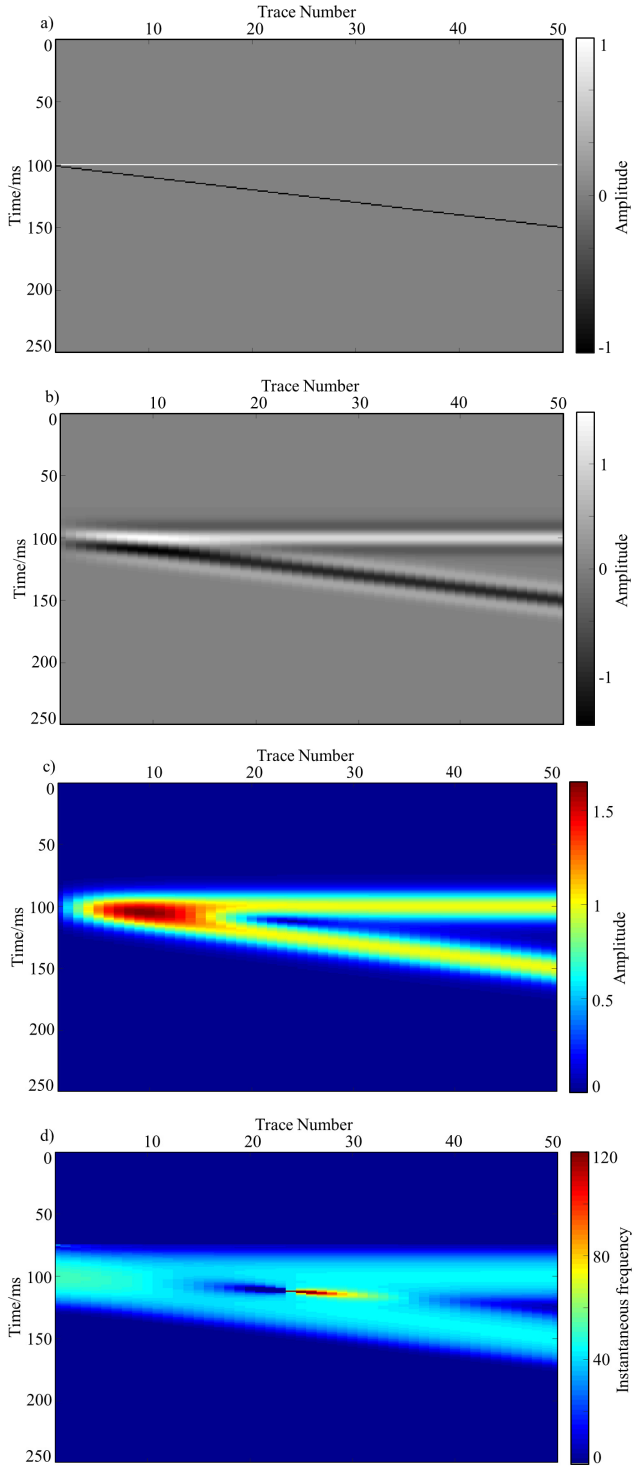

Fig. 3. Noise-free synthetic wedge model. (a) Wedge mode. (b) Synthetic wedge model. (c) IA. (d) IF. The reflectivity pair of each trace has the same magnitude with opposite polarity. The wavelet used to generate the synthetic is a 40-Hz Ricker wavelet with zero phase.

no parameter to adjust the shape and the width of the time window to obtain a flexible TF resolution. Various modified window functions are proposed to optimize the TF resolution of the ST. Mansinha *et al.* [22] adjusted the TF resolution of the ST by dividing the Gaussian time window using a user-defined scalar. Mcfadden *et al.* [23] proposed a generalized ST (GST) to avoid the restrictions on the form of the window function of the ST using several window functions, such as the exponential function with amplitude modulation by a cosine function and the exponential function with phase modulation by a cosine function. Gao *et al.* [24] proposed a GST using a modulated harmonic wave with four undetermined coefficients as the window function and applied it to thin layer detection and analysis. Pinnegar and Mansinha [25] developed a GST using a complex window function with a user-designed complex phase function and applied it to resolving time-varying waveforms. Chen *et al.* [26] proposed a modified Gaussian window with two parameters and applied the GST

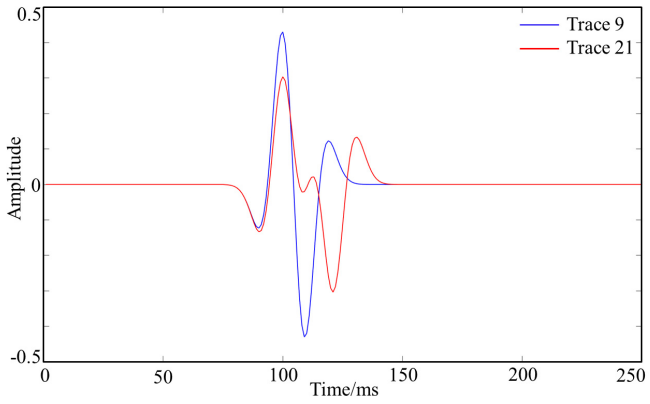

Fig. 4. 9th (blue solid line) and 21st traces (red solid line) of the seismic seismogram shown in Fig. 2(b).

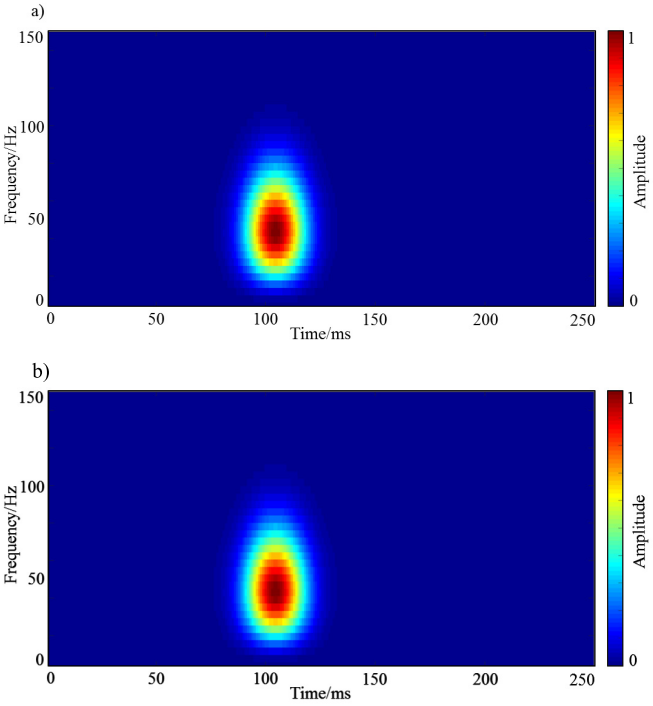

Fig. 5. Normalized TF spectra of the ninth trace. (a) Theory TF spectrum and (b) TF spectra calculated using the SAGST, respectively.

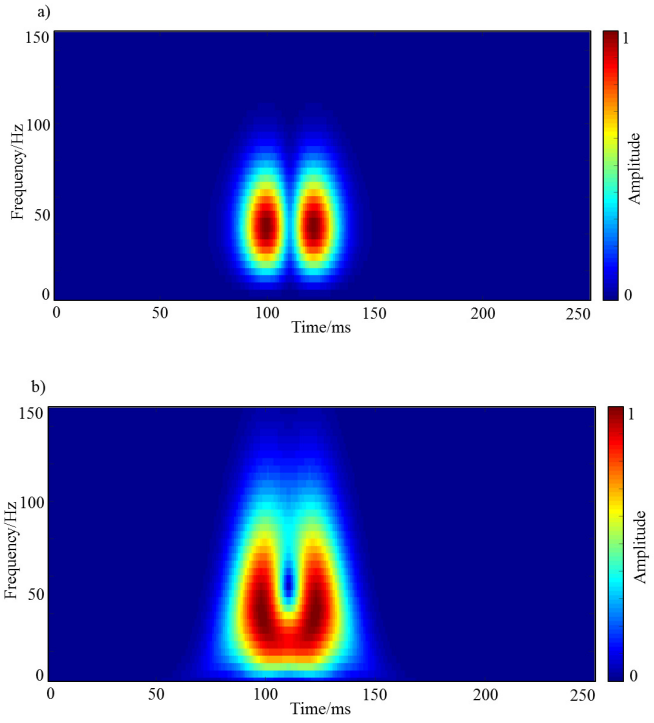

Fig. 6. Normalized TF spectra of the 21st trace. (a) Theory TF spectrum and (b) TF spectra produced using the SAGST, respectively.

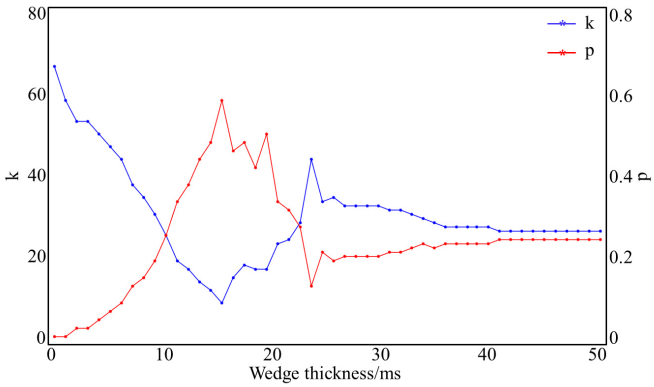

Fig. 7. Optimized k (blue star line) and p (red star line) with regard to the wedge thickness.

to estimate seismic attenuation and improve seismic time resolution. George *et al.* [27] proposed a modified ST (MST) by using a scaling function for the Gaussian window and applied it to filter time series. Wu and Castagna [28] defined an unscaled ST (UST) by removing the normalization factor of the ST and applied the UST to seismic frequency attribute extraction. Wang and Lu [29] proposed an effective amplitude-preserving GST and applied it to seismic data attenuation compensation.

The MST-based methods have more flexibility in the TF analysis. However, how to select the parameters of the MST is an unsolved question. In this paper, we propose a self-adaptive GST (SAGST) method to adjust the TF resolution within the same seismic volume adaptively. The improved GST in this paper contains two parameters to control the shape and width of the modified Gaussian window [26]. We optimize the TF resolution by flexibly selecting the two parameters of the modified Gaussian window. We use the synthetic wedge model to build a relationship template between the instantaneous frequency (IF) and optimal parameter sets, where the IF is used as an indicator of the time thickness of seismic traces. We first calculate the theory TF spectra and IF of synthetic traces of the wedge model. We then compute the TF spectrum of each trace using the GST using a set of parameters. We treat the parameter set, which has the largest similarity between the computed TF spectrum and theoretical TF spectrum, as the best parameter set. Then, we can adaptively select the parameter sets of the GST according to the IF of seismic traces in the real application. To validate our method, we first apply the proposed SAGST to noise-free and noisy synthetic traces,

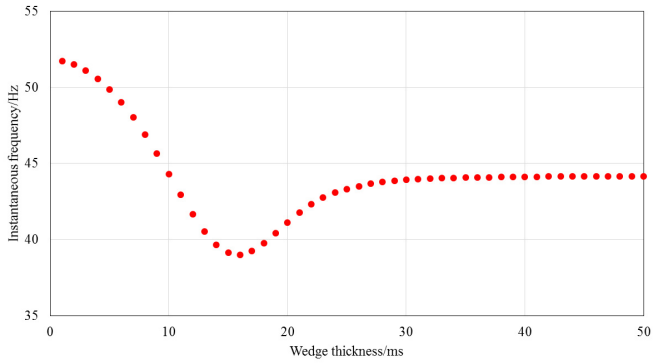

Fig. 8. IF values extracted from the wedge model at the time index of the first reflectivity.

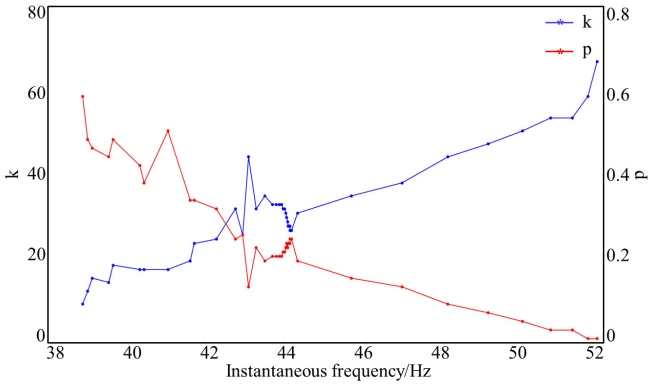

Fig. 9. Optimized k (blue star line) and p (red star line) varying with IF values.

and then use the proposed SAGST to characterize channel features of real seismic data.

The outline of this paper is as follows In Section II, we briefly review the theory of the ST and GST. We then propose the SAGST in detail in Section III. In Section IV, we give the numerical results and discussions on noise-free and noisy synthetic traces, in comparison with the proposed SAGST with the ST, MST, and GST. Furthermore, we apply the proposed SAGST to field data for characterizing channels in Section V. Finally, we summarize the conclusion of this paper in Section VI.

II. S-Transform and Generalized S-Transform

The ST [8] of a signal $s(t)$ is defined as

$$\mathrm{ST}(\tau, f) = \int_{-\infty}^{\infty} s(t) \frac{|f|}{\sqrt{2\pi}} e^{-\frac{(t-\tau)^2 f^2}{2}} e^{-i2\pi f t} dt \tag{1}$$

where t and f are the time and frequency variables, and τ denotes the localization of the frequency-dependent Gaussian window $(|f|)/(\sqrt{2\pi})e^{-((t-\tau)^2 f^2)/(2)}$. Note that the standard deviation of the Gaussian window is $\sigma(f) = 1/|f|$, which has an inverse relationship with the frequency variable f. Therefore, the ST achieves a high-frequency resolution at low frequencies and obtains a high time resolution at high frequencies. We rewrite (1) into the frequency domain as follows:

$$\mathrm{ST}(\tau, f) = \int_{-\infty}^{\infty} S(\alpha + f) e^{-\frac{2\pi^2 \alpha^2}{f^2}} e^{i2\pi\alpha\tau} d\alpha, \tag{2}$$

where $S(\alpha)$ is the Fourier transform of the analyzed signal $s(t)$, and α is the frequency variable. Equations (1) and (2) indicate that there are no parameters to adjust the shape and size of the Gaussian window. Hence, the ST is not suitable for the nonstationary signal analysis.

To adjust the Gaussian window of the ST flexibly, Chen *et al.* [26] introduced two parameters to control the size and shape of the Gaussian window and developed a GST. The modified Gaussian window is expressed as

$$g(t) = \frac{k|f^p|}{\sqrt{2\pi}} e^{-\frac{k^2 f^{2p} t^2}{2}} \tag{3}$$

where k and p are parameters working together to control the size and shape of the Gaussian window. Fig. 1(a) and (b) illustrates the width of the modified widow as a function of k and p in the time domain and frequency domain, respectively. The maximum width of the window shown in Fig. 1(a) and (b) has been normalized to one. Fig. 1(a) indicates that the window width in the time domain decreases with resolution using a small k. Fig. 1(b) indicates that the window width in the time domain increases with a decreasing p. Therefore, we obtain an improved time resolution using a large p. Then, the GST [26] is denoted as

$$\mathrm{GST}(\tau, f) = \int_{-\infty}^{\infty} s(t) \frac{|kf^p|}{\sqrt{2\pi}} e^{-\frac{(t-\tau)^2 (kf^p)^2}{2}} e^{-i2\pi f t} dt. \tag{4}$$

Equation (4) indicates that the GST can be reduced to the ST when we set $k = 1$ and $p = 1$. Equation (4) also indicates that we can optimize the TF resolution by setting the two parameters set (k, p) properly. We rewrite (4) into frequency domain as

$$\mathrm{GST}(\tau, f) = \int_{-\infty}^{\infty} S(\alpha + f) e^{-\frac{2\pi^2 \alpha^2}{(kf^p)^2}} e^{i2\pi\alpha\tau} d\alpha. \tag{5}$$

Obviously, the modified window function of the GST satisfies the admissibility condition of the unit area

$$\int_{-\infty}^{\infty} \frac{k|f^p|}{\sqrt{2\pi}} e^{-\frac{k^2 f^{2p} t^2}{2}} d\tau = 1. \tag{6}$$

The normalization condition guarantees the energy conservation and invertibility of the GST. By integrating the TF spectrum over time axis, the relationship between the Fourier spectrum of $s(t)$ and the TF spectrum of the GST is expressed as

$$\int_{-\infty}^{\infty} \mathrm{GST}(\tau, f) d\tau = S(f), \tag{7}$$

where $S(f)$ is the Fourier transform of $s(t)$. Then, the analyzed signal $s(t)$ is reconstructed by the GST coefficients simply as

$$s(t) = \int_{-\infty}^{\infty} \int_{-\infty}^{\infty} \mathrm{GST}(\tau, f) d\tau df. \tag{8}$$

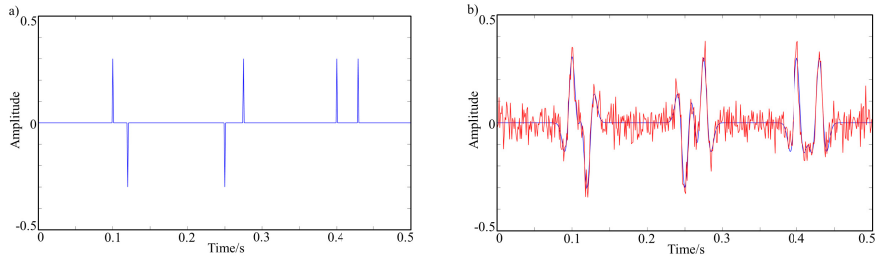

Fig. 10. Synthetic seismic trace example. (a) Reflectivity. (b) Noise-free trace (blue line) and noisy trace (red line). The added noise in our application is the Gaussian white noise. The SNR equals 5 dB. There are three reflection sets in this synthetic model. Both the first and second sets contain two reflectivities with an opposite magnitude of 0.3. The third set contains two reflectivities, both with a magnitude of 0.3. The time thicknesses of the first, second, and third pairs are 20, 25, and 30 ms, respectively.

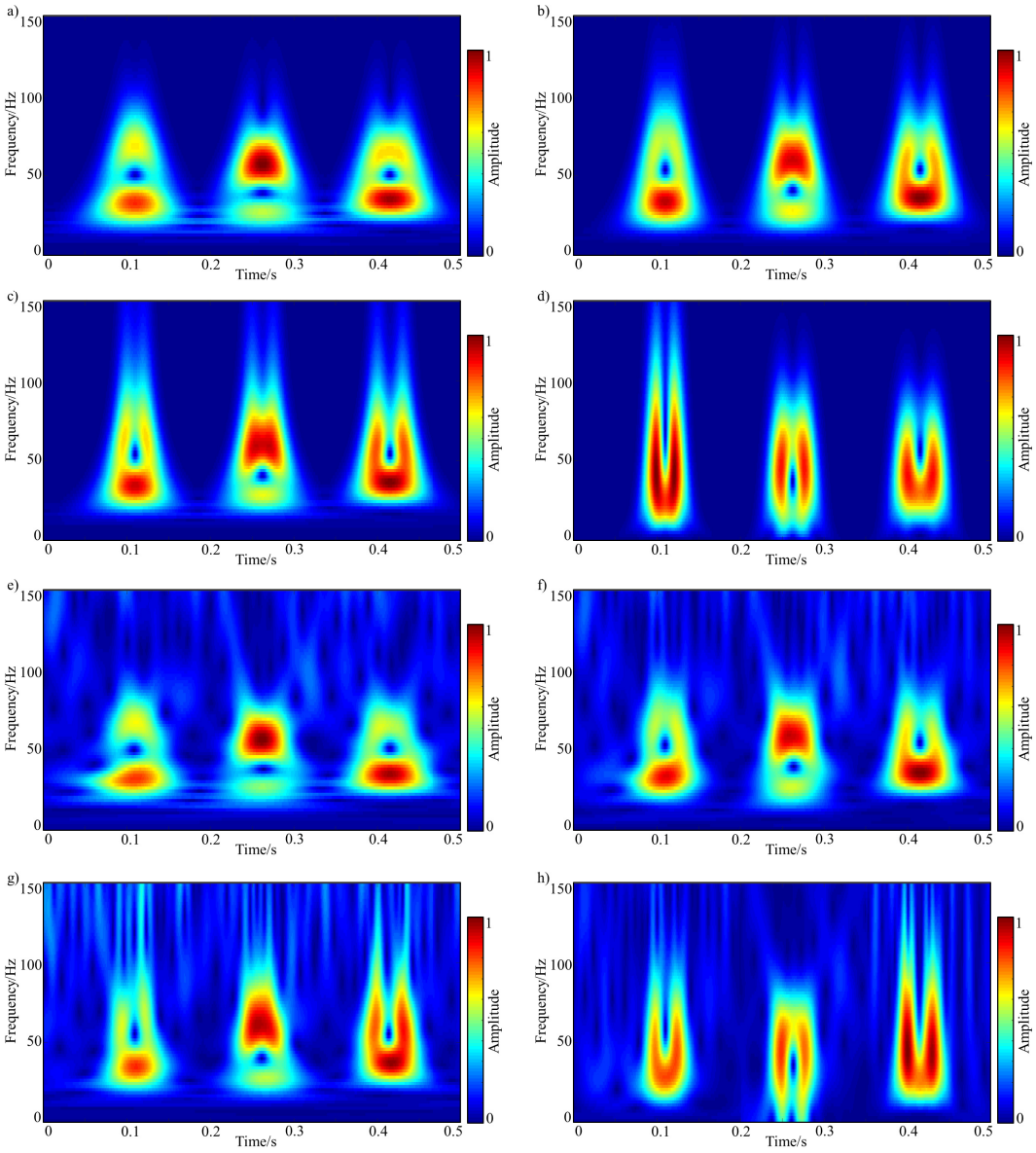

Fig. 11. TF spectra of the noise-free and noisy seismic synthetic traces. Noise-free TF spectra calculated by (a) ST, (b) MST, (c) GST, and (d) SAGST, respectively. Noisy TF spectra calculated by (e) ST, (f) MST, (g) GST, and (h) SAGST, respectively. The parameters for the MST and GST are 1.2, 5 and 1.2, 1.2 in this paper.

III. Self-Adaptive Generalized S-Transform

Equations (4) and (5) indicate the possibility of using the GST to achieve a flexible TF resolution. Fig. 2 shows the workflow of the proposed SAGST. Our research aims to obtain the "theory TF spectrum" of seismic traces using the SAGST and regard the "theory TF spectrum" as the optimized TF representation of seismic traces. The "theory TF spectrum" is a function of the time thickness and source

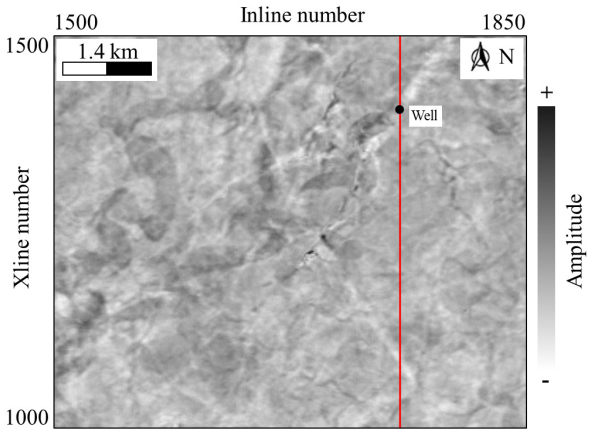

Fig. 12. Fig. 12. Horizontal slice of 3-D seismic data. Red line: location of Inline 1720.

wavelet. Note that we present the calculation of the theory TF spectrum in detail in the Appendix in this paper. Our workflow consists of three main steps. The first step is building a relationship between the parameter set of the GST and the time thickness of the thin layer. The second step is first finding the relationship between the time thickness and IF values of seismic traces and then build a relationship between the parameter set of the GST and IF values. Our last step is flexibly selecting the proper parameter set of the GST according to the IF values of seismic traces in the TF decomposition.

We use the synthetic wedge model to construct our "theory TF spectrum" template with different time thicknesses. We first compute the TF spectrum of the first trace of the wedge model using different parameter sets (k, p). We next compute and compare the similarity between the "theory TF spectrum" and TF spectrum generated using the SAGST. The parameter set (k, p) with the highest similarity is regarded as the optimal parameter set for the first trace. We repeat the same procedure to find the optimal parameter sets for all the traces with different time thicknesses in the wedge model. In this manner, we build a direct unique relationship between the parameter set (k, p) and the time thickness. Note that IF is a function of the time thickness of the wedge model [30], [31]. We finally use the IF as an indicator of the time thickness of seismic traces and choose corresponding optimized parameter set (k, p) adaptively.

Fig. 3(a) and (b) shows the reflectivity and synthetic wedge model, respectively. The reflectivity model is comprised of the reflectivity pair with different time thicknesses. The reflectivity pair of each trace has the same magnitude with opposite polarity. The wavelet used to generate the synthetic model is a 40-Hz Ricker wavelet with zero phase. Fig. 3(c) and (d) shows the instantaneous amplitude (IA) and IF of the synthetic seismogram shown in Fig. 3(b), respectively. Fig. 4 shows the 9th (blue solid line) and 21st (solid red line) traces of the synthetic seismogram in Fig. 3(b). The time thicknesses of the 9th and 21st traces are 9 and 21 ms, respectively. Figs. 5(a) and 6(a) show the theoretical TF spectra of the 9th and 21st traces. Our next step is finding the parameter set (k, p) from the user to define the parameter range. Parameter k ranges from 1 to 100 with an increment of 1. Parameter p ranges from 0.01 to 2 with an increment of 0.01. Figs. 5(b) and 6(b) show the closest TF spectra produced by the GST for the TF spectra shown in Figs. 5(a) and 6(a), respectively. The corresponding optimized parameter sets (k, p) for the 9th and 21st traces are (35, 0.16) and (24, 0.34), respectively. Fig. 7 shows the optimized parameter set (k, p) varying with different time thicknesses of the wedge model. The blue star line in Fig. 7 shows the relationship between the parameter k and the time thickness of the wedge model. The red star line in Fig. 7 shows the relationship between the parameter p and the time thickness of the wedge model.

Fig. 8 shows the extracted IF values from the wedge model at the time index of the first reflectivity. Note that we have a unique relationship between the IF values and seismic thicknesses if the time thicknesses are smaller than 30 ms. We conclude that the IF is associated with the seismic thickness, and the IF values of seismic traces can be used as the indicator of seismic thicknesses. Fig. 9 shows the optimized parameter set (k, p) with varying IF values. Finally, we can properly select the parameter set (k, p) according to the IF values in the TF decomposition. In real applications, we first calculate the 3-D seismic IF volume using the 3-D seismic data [31]. Then, we select the parameter set (k, p) based on the calculated IF volume and implement the SAGST to the 3-D seismic data. At last, we use the spectral decomposition of 3-D seismic data to characterize features of fluvial channels with different thicknesses.

IV. Synthetic Data Examples

To test the effectiveness and stableness of the proposed SAGST, we first apply it to noise-free and noisy synthetic traces. Fig. 10(a) shows the reflectivity, and Fig. 10(b) shows the noise-free (blue line) and noisy (red line) synthetic trace. The added noise in our application is the Gaussian white noise, and the SNR is 5 dB. There are three reflection sets in this synthetic trace. The first and second sets contain two reflection coefficients with an opposite magnitude of 0.3. The third set contains two reflection coefficients with the same magnitude of 0.3. The time thicknesses of the first, second, and third pairs are 20, 25, and 30 ms, respectively. We use a zero-phase 40-Hz Ricker wavelet to generate the synthetic trace, indicated by the blue line in Fig. 10(b). To illustrate the advantages of our method, we compare the TF spectra computed using the ST, MST [27], and GST [26] in synthetic testing. The parameters for the MST and GST are (1.2, 5) and (1.2, 1.2) in this paper. Fig. 11(a)–(d) shows the noise-free TF spectra calculated by the ST, MST, GST, and SAGST, respectively. Unfortunately, the TF spectrum calculated by the ST is smeared to a certain degree for all the reflection pairs. The TF spectra calculated by the MST and GST almost distinguish the third pair. The TF spectrum computed using the SAGST distinguishes all three pairs clearly. Fig. 11(e)–(h) shows the TF spectra of the noisy synthetic trace calculated by the ST, MST, GST, and SAGST, respectively. Note that the

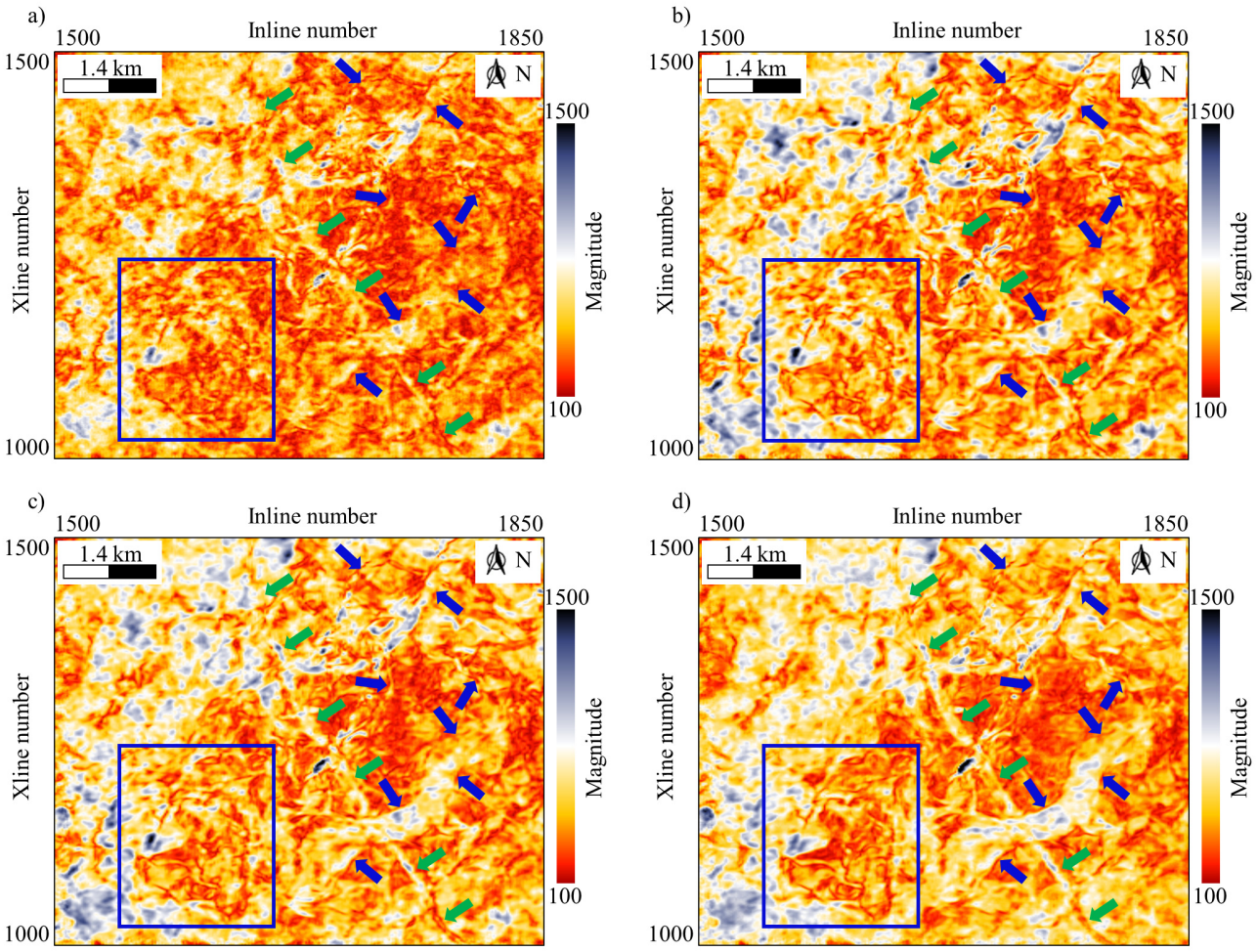

Fig. 13. Constant frequency slices at horizon T0. The 40-Hz horizon slices calculated using (a) ST, (b) MST, (c) GST, and (d) SAGST, respectively. Green and blue arrow: channels with different thicknesses.

SAGST is still superior to the other methods in the thin bed identification in a noisy environment. Both noise-free and noisy synthetic seismic examinations illustrate that the SAGST is superior to the ST, MST, and GST in detecting thin beds.

V. Offshore Seismic Data

To further demonstrate the superiority of the proposed SAGST, we compare the capability of channel detection using TF spectra computed using different TF methods. The seismic survey used in this paper is located at the Yellow River delta area of Bohai Bay Basin, east of China. The depositional settings of the primary reservoirs (the Middle Miocene Minghuazhen Formation) are dominated by stacked fluvial channels and delta systems in several depositional cycles [32], [33]. These depositional facies make seismic interpretation and reservoir characterization of this field very difficult. Therefore, we apply TF algorithms to illustrate more depositional details of the stacked fluvial channels.

The 3-D seismic data used in this paper are a cropped seismic volume. The Inline number ranges from 1500 to 1850, whereas the Xline number ranges from 1000 to 1500. The sample rate of the seismic data is 2 ms. Fig. 12 shows the horizontal slice of the 3-D seismic data at the horizon T0. The red line indicates the location of Inline 1720. There is a well located at Inline 1720, indicated by the dark spot. The fluvial channels are difficult to follow on the horizon slice of seismic data shown in Fig. 12. Fig. 13(a)–(d) shows the 40-Hz spectral slices calculated using the ST, MST [27], GST [26], and the proposed SAGST, respectively. Note that the parameters for the MST and GST are (1.2, 5) and (1.2, 1.2) in this paper, respectively. The spectral component computed using the ST cannot characterize the channels due to its low TF resolution. The MST and GST improve the TF resolution and characterize the channels more clearly than the ST. However, the SAGST describes the channels with different thicknesses more clearly and continuously than the other three TF algorithms. The green arrows indicate a narrow and continuous channel at this seismic area, whereas the blue arrows indicate the edges of the channels with different thicknesses. The blue rectangle indicates superimposed channels in the seismic area.

We further use the red-green-blue (RGB) blending technique to characterize channel edges by combining three spectral components together into one map [33], [34]. Fig. 14(a)–(d) shows the RGB blending images of the 20-, 40-, and 70-Hz spectral slices calculated using the ST, MST, GST, and the

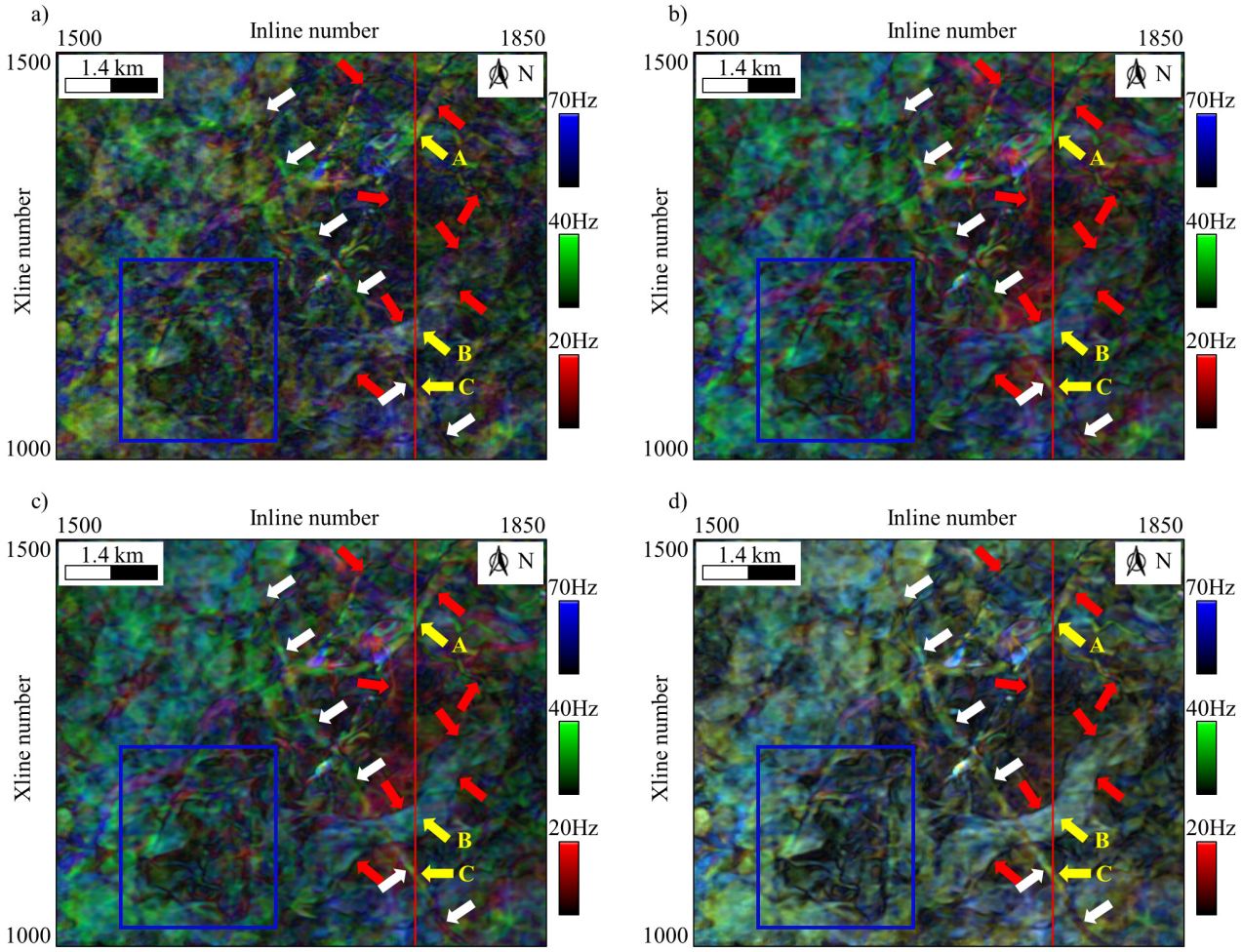

Fig. 14. RGB blending images using the 20, 40, and 70-Hz spectral components. RGB blending images calculated using (a) ST, (b) MST, (c) GST, and (d) SAGST, respectively. Three yellow arrows with labels A, B, and C indicate three distinct channels located at Inline 1720.

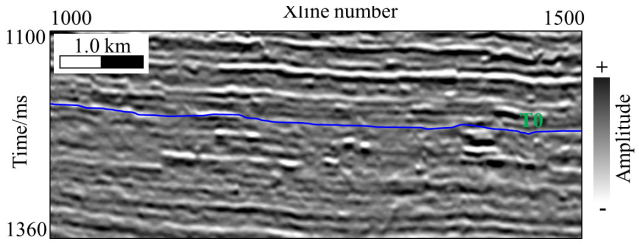

Fig. 15. 2-D seismic data at Inline 1720.

proposed SAGST, respectively. All RGB blending images highlight the distribution of wide channels. However, the RGB blending image produced using the SAGST is superior to those calculated using the ST, MST, and GST in characterizing the channel edges indicated by the red arrows. The continuous channel indicated by the white arrows in Fig. 14(d) is more continuous than those in Fig. 14(a)–(c). The three yellow arrows with labels A, B, and C indicate three distinct channels with different thicknesses, located at Inline 1720.

To better view the optimized TF resolution, we compare the decomposed frequency components on a 2-D vertical seismic section with Inline number 1720, indicated by red lines in Figs. 12 and 14. Fig. 15 shows the 2-D seismic data of Inline 1720. The blue curve in Fig. 15 denotes the horizon T0. Fig. 16(a)–(d) shows the 40-Hz spectral components calculated using the ST, MST, GST, and SAGST, respectively. The blue lines in Fig. 16 are the horizon T0, whereas the green curves in Fig. 16 are the gamma curves. The gamma curves demonstrate that the depositional settings of the primary reservoirs are dominated by the stacked fluvial channels and delta systems in several depositional cycles. In addition, three green arrows with labels A, B, and C indicate three distinct channels at this vertical seismic section, which are indicated by the yellow arrows with labels A, B, and C in Fig. 14. Note that we have smeared channel features in Fig. 16(a). The MST and GST highlight the channels due to its improved TF resolution. Obviously, the SAGST characterizes the edges of the channels more clearly than the ST, MST, and GST. Furthermore, the channel features highlighted by SAGST are more continuous than those calculated by the ST, MST, and GST. The field data applications demonstrate the effectiveness of the proposed SAGST in characterizing the edges of channels with different thicknesses.

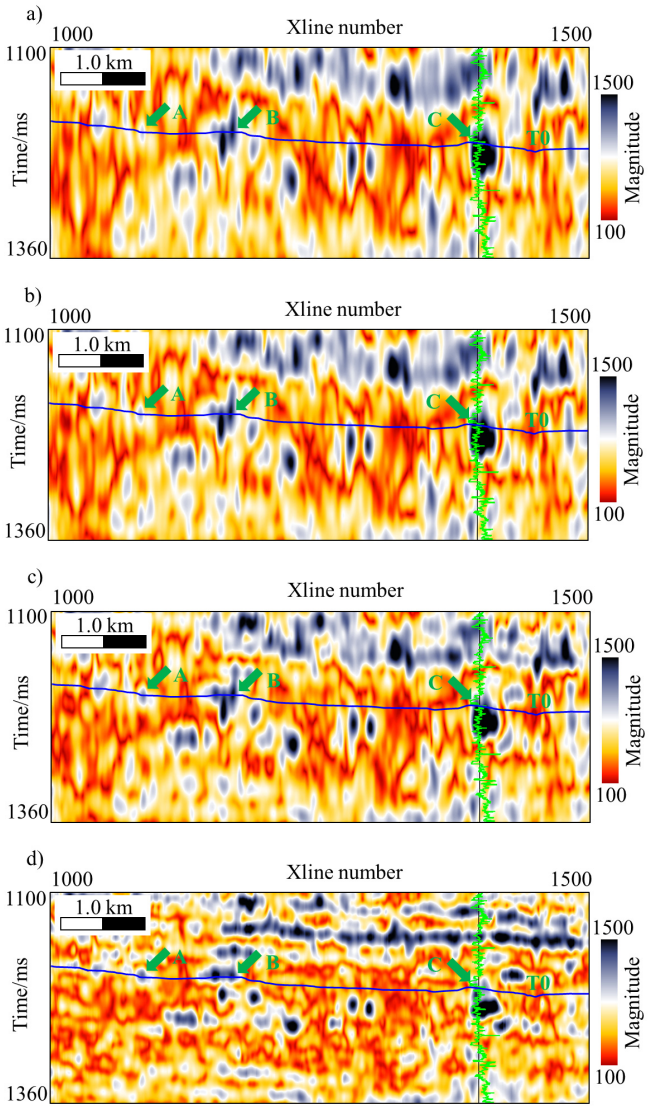

Fig. 16. 40-Hz spectral components for Inline 1720. The 40-Hz spectral components calculated using (a) ST, (b) MST, (c) GST, and (d) SAGST, respectively. Blue line: horizon T0. Three green arrows with labels A, B, and C indicate three distinct channels at this vertical seismic section, which are indicated by three yellow arrows with labels A, B, and C in Fig. 14.

VI. Conclusion

In this paper, we propose an SAGST to optimize the TF representation of seismic traces. We use two parameter sets to achieve an optimized TF spectrum calculated using the GST. We first build the relationship between the parameter set (k, p) of the GST and seismic thickness using a synthetic wedge model. We then select a parameter set flexibly using the IF values of the seismic trace. The testing on noise-free and noisy synthetic traces demonstrates the effectiveness and stableness of the proposed SAGST in optimizing the TF resolution of analyzed signals. The field data further show that the proposed SAGST characterizes features of fluvial channels with different thicknesses more clearly and accurately, especially fluvial channel edges.

This paper presents a novel workflow to select parameters of TF algorithms with parameters adaptively. The proposed SAGST achieves an improved TF representation with a high TF resolution. In the future, we can generalize the proposed workflow to other TF algorithms with adjustable parameters easily and apply them to seismic TF analysis. Note that the calculation time of the proposed SAGST is several times of the GST. Hence, we aim to improve the calculation efficiency of the proposed SAGST for further research.

Appendix

Calculation of the Theory Time–Frequency Representation

A true joint TF distribution $F(t, \omega)$ must satisfy the following two fundamental marginal requirements for the analyzed seismic signal $s(t)$, defined in (A1) and (A2)

$$\int_{-\infty}^{\infty} F(t, \omega) d\omega = |s(t)|^2 \tag{A1}$$

$$\int_{-\infty}^{\infty} F(t, \omega) dt = |S(\omega)|^2 \tag{A2}$$

In this paper, we introduce the positive distribution function to calculate the theory TF representation [31]. We first denote the analyzed seismic signal as $s(t)$ and its Fourier spectrum as $S(\omega)$. The positive distribution of the seismic analyzed signal is then defined in (A3)

$$F(t, \omega) = |s(t)|^2 |S(\omega)|^2 \{1 + c\rho(x(t), y(\omega))\} \tag{A3}$$

where c is a numerical constant and must be in the range $\{-1/l_2 \le c \le 1/l_1\}$. l_1 and l_2 are the absolute minimum and maximum of $\rho(x(t), y(\omega))$. In addition, we have

$$\rho(x(t), y(\omega)) = h(x, y) - h_1(x) - h_2(y) + 1 \tag{A4}$$

$$x(t) = \int_{-\infty}^{t} |s(t')|^2 dt \text{ and } y(\omega) = \int_{-\infty}^{\omega} |S(\omega')|^2 d\omega \tag{A5}$$

where $h(x, y)$ is any positive function of the variables x and y in the unit square $\{0 \le x, y \le 1\}$ and normalized to one. $h_1(x)$ and $h_2(x)$ are the margins of $h(x, y)$, defined in (A6)

$$h_1(x) = \int_0^1 h(x, y) dy \text{ and } h_2(y) = \int_0^1 h(x, y) dx \tag{A6}$$

In the following, we aim to prove that the proposed positive TF distribution in (B3) satisfies the marginal requirements in (A1) and (A2). We first generate the analytical seismic signal $s_a(t)$ of the analyzed seismic signal $s(t)$. The analytical seismic signal $s_a(t)$ is defined in (A7)

$$s_a(t) = s_R(t) + i s_I(t) \tag{A7}$$

where $s_R(t) = s(t)$ and $s_I(t) = Im[s_a(t)] = H[s_R(t)] = (1)/(\pi) \int_{-\infty}^{\infty} (s_R(\tau))/(t - \tau) d\tau$. Then, we have

$$\begin{aligned} &\int_{-\infty}^{\infty} F(t, \omega) d\omega \\ &\quad = |s_a(t)|^2 \int_{-\infty}^{\infty} |S_a(\omega)|^2 \{1 + c\rho(x, y)\} d\omega \\ &\quad = |s_a(t)|^2 + c|s_a(t)|^2 \int_{-\infty}^{\infty} |S_a(\omega)|^2 \rho(x, y) d\omega \end{aligned} \tag{A8}$$

where $S_a(\omega)$ is the Fourier spectrum of the analytical seismic signal $s_a(t)$ In addition, we have

$$\begin{aligned}\int_{-\infty}^{\infty}|S_a(\omega)|^2\rho(x,y)d\omega &= \int_0^1 \rho(x,y)dy \\ &= \int_0^1 [h(x,y)-h_1(x)-h_2(y)+1]dy \\ &= h_1(x)-h_1(x)-1+1 \\ &= 0 \end{aligned} \tag{A9}$$

Substituting (A9) into (A8), we obtain (A1) easily. Similar for (A2).

ACKNOWLEDGMENT

The authors would like to thank the Research Institute of China National Offshore Oil Corporation (CNOOC) for providing the license for the seismic data volume used in this paper. They would also like to thank the editor and reviewers for their valuable comments, which improve the presentation of this paper. They would also like to thank Dr. B. Zhang for inspiring discussions.

REFERENCES

[1] S. Sinha, P. Routh, P. Anno, and J. Castagna, "Spectral decomposition of seismic data with continuous-wavelet transform," *Geophysics*, vol. 70, no. 6, pp. P19–P25, Nov. 2005.

[2] D. Gabor, "Theory of communication," *J. Inst. Elect. Eng.*, vol. 93, no. 26, pp. 429–441, Nov. 1946.

[3] J. B. Allen, "Short term spectral analysis, synthesis, and modification by discrete Fourier transform," *IEEE Trans. Acoust., Speech Signal Process.*, vol. ASSP-25, no. 3, pp. 235–238, Jun. 1977.

[4] L. Cohen, *Time-Frequency Analysis*. Upper Saddle River, NJ, USA: Prentice-Hall, 1995.

[5] W. Lu and F. Li, "Seismic spectral decomposition using deconvolutive short-time Fourier transform spectrogram," *Geophysics*, vol. 78, no. 2, pp. V43–V51, Jan. 2013.

[6] I. Daubechies, "The wavelet transform, time-frequency localization and signal analysis," *IEEE Trans. Inf. Theory*, vol. 36, no. 5, pp. 961–1005, Sep. 1990.

[7] I. Daubechies, *Ten Lectures on Wavelets*. Philadelphia, PA, USA: SIAM, 1992.

[8] R. G. Stockwell, L. Mansinha, and R. P. Lowe, "Localization of the complex spectrum: The S transform," *IEEE Trans. Signal. Process.*, vol. 44, no. 4, pp. 998–1001, Apr. 1996.

[9] E. P. Wigner, "On the quantum correction for thermodynamic equilibrium," *Phys. Rev.*, vol. 40, no. 5, p. 749–759, Jan. 1932.

[10] J. Ville, "Théorie et application dela notion de signal analytique ," *Cables Transmiss.*, vol. 2, no. 1, pp. 61–74, 1948.

[11] L. Cohen, "Time-frequency distributions—A review," *Proc. IEEE*, vol. 77, no. 7, pp. 941–981, Jul. 1989.

[12] S. G. Mallat and Z. Zhang, "Matching pursuits with time-frequency dictionaries," *IEEE Trans. Signal Process.*, vol. 41, no. 12, pp. 3397–3415, Dec. 1993.

[13] J. Liu and K. J. Marfurt, "Instantaneous spectral attributes to detect channels," *Geophysics*, vol. 72, no. 2, pp. P23–P31, Jan. 2007.

[14] C. I. Puryear, O. N. Portniaguine, C. M. Cobos, and J. P. Castagna, "Constrained least-squares spectral analysis: Application to seismic data," *Geophysics*, vol. 77, no. 5, pp. V143–V167, Aug. 2012.

[15] X. Wang, B. Zhang, F. Li, J. Qi, and B. Bai, "Seismic time-frequency decomposition by using a hybrid basis-matching pursuit technique," *Interpretation*, vol. 4, no. 2, pp. T239–T248, May 2016.

[16] F. Auger and P. Flandrin, "Improving the readability of time-frequency and time-scale representations by the reassignment method," *IEEE Trans. Signal Process.*, vol. 43, no. 5, pp. 1068–1089, May 1995.

[17] I. Daubechies, J. Lu, and H.-T. Wu, "Synchrosqueezed wavelet transforms: An empirical mode decomposition-like tool," *Appl. Comput. Harmon. Anal.*, vol. 30, no. 2, pp. 243–261, Mar. 2011.

[18] N. Liu, J. Gao, Z. Zhang, X. Jiang, and Q. Lv, "High-resolution characterization of geologic structures using the synchrosqueezing transform," *Interpretation*, vol. 5, no. 1, pp. T75–T85, Nov. 2016.

[19] N. Liu, J. Gao, X. Jiang, Z. Zhang, and Q. Wang, "Seismic time–frequency analysis via STFT-based concentration of frequency and time," *IEEE Geosci. Remote Sens. Lett.*, vol. 14, no. 1, pp. 127–131, Jan. 2017.

[20] A. M. Gargoom, N. Ertugrul, and W. L. Soong, "Automatic classification and characterization of power quality events," *IEEE Trans. Power Del.*, vol. 23, no. 4, pp. 2417–2425, Oct. 2008.

[21] R. G. Stockwell, "A basis for efficient representation of the S-transform," *Digit. Signal Process.*, vol. 17, no. 1, pp. 371–393, Jan. 2007.

[22] L. Mansinha, R. G. Stockwell, and R. P. Lowe, "Pattern analysis with two-dimensional spectral localisation: Applications of two-dimensional S transforms," *Phys. A, Stat. Mech. Appl.*, vol. 239, nos. 1–3, pp. 286–295, May 1997.

[23] P. D. Mcfadden, J. G. Cook, and L. M. Forster, "Decomposition of gear vibration signals by the generalised S transform," *Mech. Syst. Signal Process.*, vol. 13, no. 5, pp. 691–707, Sep. 1999.

[24] J. Gao, W. Chen, Y. Li, and F. Tian, "Generalized S transform and seismic response analysis of thin interbedss surrounding regions by Gps," *Chin. J. Geophys.*, vol. 46, no. 4, pp. 759–768, Jul. 2003.

[25] C. R. Pinnegar and L. Mansinha, "Time-local Fourier analysis with a scalable, phase-modulated analyzing function: The S-transform with a complex window," *Signal Process.*, vol. 84, no. 7, pp. 1167–1176, 2004.

[26] X. Chen, Z. He, D. Huang, and X. Wen, "Low frequency shadow detection of gas reservoirs in time-frequency domain," *Chin. J. Geophys.*, vol. 52, no. 1, pp. 215–221, 2009.

[27] N. V. George, S. S. Sahu, L. Mansinha, K. F. Tiampo, and G. Panda, "Time localised band filtering using modified S-transform," in *Proc. Int. Conf. Signal Process. Syst.*, May 2009, pp. 42–46.

[28] L. Wu and J. Castagna, "S-transform and Fourier transform frequency spectra of broadband seismic signals," *Geophysics*, vol. 82, no. 5, pp. O71–O82, Aug. 2017.

[29] B. Wang and W. Lu, "An efficient amplitude-preserving generalized S transform and its application in seismic data attenuation compensation," *IEEE Trans. Geosci. Remote. Sens.*, vol. 56, no. 2, pp. 859–866, Feb. 2017.

[30] J. D. Robertson and H. H. Nogami, "Complex seismic trace analysis of thin beds," *Geophysics*, vol. 49, no. 4, pp. 344–352, Apr. 1984.

[31] N. Liu, J. Gao, X. Jiang, Z. Zhang, and P. Wang, "Seismic instantaneous frequency extraction based on the SST-MAW," *J. Gephpys. Eng.*, vol. 15, no. 3, pp. 995–1007, Mar. 2018.

[32] Q. Ye *et al.*, "Interpretation and reservoir characterization of a field dominated by complex fluvial channels, Bohai Bay, China," *Lead. Edge*, vol. 28, no. 3, pp. 346–352, Mar. 2009.

[33] Z. Wang, B. Zhang, J. Gao, Q. Wang, and Q. Liu, "Wavelet transform with generalized beta wavelets for seismic time-frequency analysis," *Geophysics*, vol. 82, no. 4, pp. O47–O56, 2017.

[34] N. Liu, J. Gao, B. Zhang, F. Li, and Q. Wang, "Time–frequency analysis of seismic data using a three parameters S transform," *IEEE Geosci. Remote. Sens. Lett.*, vol. 15, no. 1, pp. 142–146, Jan. 2018.

[35] L. Cohen and Y. Zaparovanny, "Positive quantum joint distributions," *J. Math. Phys.*, vol. 21, no. 4, pp. 794–796, Apr. 1980.

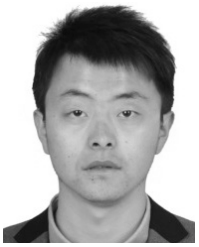

Naihao Liu received the B.S. degree in communication engineering from Jilin University, Changchun, China, in 2012, and the Ph.D. degree in information and communication engineering form Xi'an Jiaotong University, Xi'an, China, in 2018.

From 2017 to 2018, he visited the Department of Geological Sciences, University of Alabama, Tuscaloosa, AL, USA. He is currently with the School of Electronic and Information Engineering, Xi'an Jiaotong University. His research interests include machine learning, seismic time–frequency analysis, seismic attributes analysis, seismic attenuation, and reservoir characterization.

Jinghuai Gao (M'19) received the M.S. degree in applied geophysics from Chang'an University, Xi'an, China, in 1991, and the Ph.D. degree in electromagnetic field and microwave technology from Xi'an Jiaotong University, Xi'an, in 1997.

From 1997 to 2000, he was a Post-Doctoral Researcher with the Institute of Geology and Geophysics, Chinese Academy of Sciences, Beijing, China. In 1999, he was a Visiting Scientist with the Modeling and Imaging Laboratory, University of California at Santa Cruz, Santa Cruz, CA, USA. He is currently a Professor with the School of Electronic and Information Engineering, Xi'an Jiaotong University. He is also the Associate Director of the National Engineering Laboratory for Offshore Oil Exploration, Xi'an. He is also the Project Leader of the Fundamental Theory and Method for Geophysical Exploration and Development of Unconventional Oil and Gas, which is a Major Program of the National Natural Science Foundation of China under Grant 41390454. His research interests include seismic wave propagation and imaging theory, seismic reservoir and fluid identification, seismic inverse problem theory, and method.

Dr. Gao was a recipient of the Chen Zongqi Geophysical Best Paper Award in 2013. He is an Editorial Board Member of the *Journal of Chinese Journal of Geophysics*, *Applied Geophysics*, and *Chinese Science Bulletin*. He is an Associate Editor of the journal of the IEEE TRANSACTIONS ON GEOSCIENCE AND REMOTE SENSING.

Bo Zhang received the bachelor's degree from the China University of Petroleum (Huadong), Dongying, China, in 2006, the master's degree in geophysics from the Institute of Geology and Geophysics, Chinese Academy of Sciences, Beijing, China, in 2009, and the Ph.D. degree in geophysics with the Industry Supported Consortium (AASPI), University of Oklahoma, Norman, OK, USA, in 2014.

In 2014, he joined Michigan Technological University, Houghton, MI, USA, as a Visiting Assistant Professor. In 2015, he joined the University of Alabama, Tuscaloosa, AL, USA, as an Assistant Professor. His research interests include broadband seismic data processing, development and calibration of new seismic attributes, pattern recognition of geologic features on 3-D seismic data, the application of machine learning and deep learning in oil and gas exploration, and unconventional resource plays characterization.

Qian Wang, photograph and biography not available at the time of publication.

Xiudi Jiang, photograph and biography not available at the time of publication.